An Accurate Automatic Quality-Factor Tuning Scheme for Second-Order *LC* Filters

Faramarz Bahmani, *Member, IEEE*, Teresa Serrano-Gotarredona, and Edgar Sánchez-Sinencio, *Fellow, IEEE*

***Abstract*—This paper presents a scheme to accurately tune the quality factor of second-order *LC* bandpass filters. The information of the magnitude response at the center and one of the cutoff frequencies is used to tune both the amplitude and the quality factor of the filter using two independent yet interacting loops. Furthermore, the synergic interaction between the loops makes the proposed scheme stable and insensitive to the mismatch between the input amplitudes. A chip prototype was implemented in a 0.35-μm CMOS process and consumes 4.3 mA from a single 1.3-V supply. Measurement results show that at 1.97 GHz the quality factor is tunable from 60 to 220 while the amplitude is tunable between -15 and 0 dBm with worst case quality factor and amplitude tuning accuracies of 10% and 7%, respectively.**

Q Q

***Index Terms*—Automatic -tuning, CMOS circuits, *LC* band-pass filter, -enhancement.**

I. Introduction

DURING the last few years, there has been an increasing demand for wireless communication equipment. There are some points in the signal processing chain of such equipment where bandpass integrated filters are required. These filters have to operate at frequencies in the gigahertz range [1]–[3].

Traditionally, gigahertz filters were implemented off-chip with lumped *RLC* components, but recently, the increasing demand for portable low-cost radio frequency front ends has motivated the emergence of integrated *LC* filters [3]. However, the implementation of integrated *LC* filters continues to present a challenge. The low quality factor of on-chip inductors requires the introduction of active circuitry implementing a negative resistance to compensate for the losses associated with the inductance [4]. Furthermore, the large unpredictable variations in component values and parasitics of monolithic implementations produce large variations in the resonance frequencies and filter quality factors. These variations make the filter completely useless unless some kind of tuning can be done after fabrication. Even in this scenario, the variations in temperature and operating conditions make it necessary to include automatic tuning circuitry to have a practical commercial product.

Automatic frequency tuning schemes for *LC* filters have already been developed [3], [5], and [6]. They employ the same techniques used for G_m–C filters [7]–[11]. A master filter in a voltage-controlled oscillator (VCO) configuration is used to sense the oscillation frequency and a phase-locked loop (PLL) is used to lock the oscillation frequency of the VCO to the desired reference frequency. However, the quality factor (Q) tuning scheme of *LC* filters cannot follow the same principles of G_m–C filters due to the lack of a simple relation between Q and amplitude response at the center frequency.

In this paper, we introduce a technique for automatic tuning of the quality factor of the *LC* filters which relies neither on the phase information of the filter nor the exact value of the amplitude gain at the center frequency. The quality-factor tuning is achieved based on the adjustment of the amplitude response of the filter at the center and one of the cutoff frequencies. Furthermore, since most of the information is processed at very low frequencies good accuracies are obtained. For example it can achieve an accuracy of 1.9% for $Q = 50$. This technique is validated through experimental results. We will present the development of Q-tuning architectures to reach the optimal proposed stable architecture.

The paper is structured as follows. In Section II, the second-order *LC* bandpass filter architecture and issues associated with its tuning are described. Previous tuning schemes reported in the literature are reviewed in Section III. The proposed automatic Q-tuning scheme is also presented in Section III. The potential tuning errors limiting the accuracy of the proposed technique are discussed in Section IV. The experimental results of the fabricated chip are presented in Section V. In Section VI, conclusions are given.

II. *LC* Filter Architecture

A parallel *LC* tank can be used as a second-order resonator. Due to the losses associated with the integrated spiral inductors, the achievable quality factor in RF range is limited. Thus, to implement an on-chip narrow band *LC* filter, positive feedback is needed for Q-enhancement which is equivalent to adding a negative resistance to compensate for the losses [4]. Serial parasitic resistance of the on-chip inductors, low-Q diode junction capacitances, and the lossy substrate are the main sources of loss in the *LC* tank. The inductor resistance is the dominant loss. The center frequency ω_0 and the quality factor Q of the resonator in Fig. 1 can be described as

$$\omega_0 = \frac{1}{\sqrt{LC}}\sqrt{1 - G_{\text{neg}}R_L} \tag{1}$$

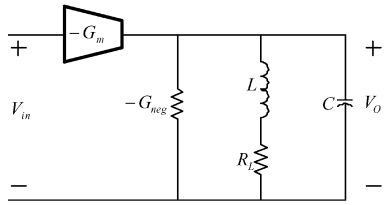

Fig. 1. Linear model of a Q-enhanced *LC* tank.

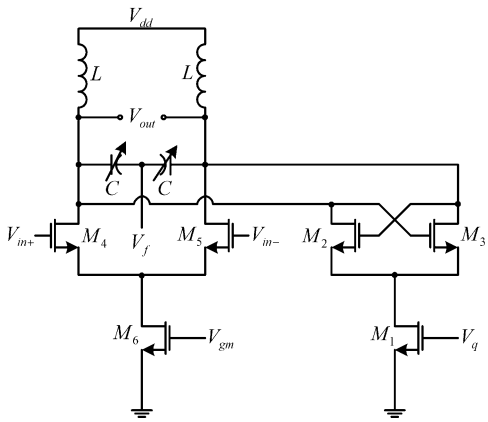

Fig. 2. Q-enhanced *LC* bandpass filter.

$$Q = \frac{1}{1 - G_{\text{neg}} Q_0^2 R_L} Q_0 \tag{2}$$

where $Q_0 = L\omega_0/R_L$. The circuit implementation of the negative transconductance, G_{neg}, is going to be explained later on in this section.

Note that (2) is valid only around the *LC* tank's resonant frequency, due to the fact that the equivalent series resistance R_L from the inductor loss varies with frequency.

The series combination of the inductor L and its loss R_L can be modeled as a parallel combination of $L_P = L(1+1/Q_0^2)$ and $R_P = R_L(1+Q_0^2)$ [12]. If the inductor quality factor Q_0 is large enough then, $L_P \approx L$ and $\omega_0^2 \approx 1/LC$. Thus, the frequency response of the filter in Fig. 1 can be approximated as

$$\begin{aligned} H(s) = \frac{V_o(s)}{V_{\text{in}}(s)} &\cong \frac{-(G_m/C)s}{s^2 + \frac{G_p - G_{\text{neg}}}{C} s + \frac{1}{LC}} \\ &= \frac{-A_0 \frac{\omega_0}{Q} s}{s^2 + \frac{\omega_0}{Q} s + \omega_0^2} \end{aligned} \tag{3}$$

where $G_p = 1/R_p, A_0 = G_m/(G_P - G_{\text{neg}}) = G_m Q\sqrt{L/C}$ and $Q = \sqrt{C/L}/(G_P - G_{\text{neg}})$.

Fig. 2 shows the circuit implementation of a second-order Q-enhanced *LC* filter. The center frequency tuning is achieved through varactors which are pMOS transistors implemented in separate wells (in an n-well technology) and with their drain/source terminals connected together to the well terminal. The capacitance seen by the gate is adjusted by changing the voltage V_f and exploiting the variation of the gate capacitance when the transistor goes from weak inversion to the accumulation region [2].

The negative transconductance G_{neg} is implemented by transistors M1–M3. Transistors M2–M3 form a differential pair with its output nodes cross-connected to its inputs, while M1 provides the bias current I_q. The transconductance associated with this cross-coupled pair can be expressed as $G_{\text{neg}} = \sqrt{\mu C_{\text{ox}}(W/L)_{2,3} I_q}$ [13]. By substituting in this equation the expression of the bias current $I_q = 0.5\mu C_{\text{ox}}(W/L)_1(V_q - V_T)^2$, the following expression for the negative transconductance, G_{neg}, as a function of the bias voltage V_q can be obtained

$$G_{\text{neg}} = \beta_q(V_q - V_T) \tag{4}$$

where $\beta_q = \mu C_{\text{ox}}\sqrt{0.5(W/L)_{2,3}(W/L)_1}$ and $(W/L)_i, i = 1, 2$ and 3 refer to the (W/L) ratios of M_i in Fig. 2. In the above equations μ, C_{ox}, and V_T have their usual meaning of mobility, oxide capacitance density and threshold voltage of the MOS transistors.

Observe from (2) and (4) that the quality factor of the filter can be tuned by adjusting the bias voltage V_q.

The control voltage V_{gm} changes the transconductance G_m of the input differential pair M_4-M_5 thus, changing the peak amplitude gain A_0 of the filter while keeping the Q invariant. Note that G_m as a function of V_{gm} can be expressed as

$$G_m = \beta_m(V_{\text{gm}} - V_T) \tag{5}$$

where $\beta_m = 0.5\ \mu C_{\text{ox}}\sqrt{0.5(W/L)_{4,5}(W/L)_6}$ and $(W/L)_{4,5}$ and $(W/L)_6$ refer to the (W/L) ratios of $M_{4,5}$ and M_6 in Fig. 2, respectively.

Thus, using (4) and (5), the peak amplitude gain A_0, defined in (3), can be expressed as

$$A_0 = \frac{G_m}{G_P - G_{\text{neg}}} = \frac{2\beta_m(V_{\text{gm}} - V_T)}{G_P - \beta_q(V_q - V_T)}. \tag{6}$$

In a similar way, the quality factor Q can be expressed as

$$Q = \sqrt{\frac{C}{L}} \frac{1}{G_P - \beta_q(V_q - V_T)}. \tag{7}$$

III. Automatic Quality-Factor Tuning

A. Existing Quality-Factor Tuning Techniques

The traditional Q-tuning schemes reported for G_m–C filters [9]–[11], [14]–[16] are not applicable to *LC* filters mainly because most of them rely on the fact that $H(j\omega_0) = Q$. Currently, available Q-tuning schemes for high frequency *LC* filters manipulate the frequency response of the filter in a digital [17]–[20] or an analog [6] feedback loop.

In [17] the quality-factor tuning is achieved by converting the *LC* filter to an oscillator and then varying the negative transconductance until the desired (stable) Q is achieved. However, this technique relies on the assumption that the variation of the negative transconductances in the filter and the oscillator is constant which is valid only if a relatively high quality-factor inductor is used in the resonator.

In [18], the center frequency and the quality-factor tuning are achieved by comparing the amplitude gain at three different frequencies. Low accuracy of the gain comparison at high frequencies and relying on the matching between the sampling times of

the error signal at different frequencies are the main drawbacks of this technique.

In [19], a digital tuning scheme based on the phase comparison of the filter at different frequencies is presented. However, finite resolution of the needed frequency synthesizer, phase offset and parasitic poles and zeros of the filter limit its performance especially for high frequency applications.

The scheme presented in [20] is based on direct characterization of the complete frequency response of the filter, and it is not adaptable to automatic Q-tuning. Finally, the VCO-based Q-tuning approach presented in [6] is a significant advance in the theory of automatic Q-tuning of *LC* filters. It varies the negative transconductance to tune a number of *LC* resonators to behave as ideal (loss-less) resonators based on a master-slave approach. However, the fact that the negative transconductance added to the *LC* resonators compensate the losses of the passive components only at one particular frequency imposes restriction on wider frequency range filters.

B. Proposed Quality-Factor Tuning Scheme

The proposed scheme in this work independently tunes the quality factor Q and the amplitude gain A_0 of the filter at its center frequency, while using information of the transfer function at two different frequencies. Assuming that these two frequencies are the center (ω_0) and one of the -3-dB cutoff frequencies (ω_L), an iterative scheme to tune the Q and the gain of the filter at the center frequency is proposed. Based on the fact that $|H(j\omega_0)| = A_0$ and $|H(j\omega_{3\text{ dB}})| = A_0/\sqrt{2}$, the following results can be obtained:

$$\omega_L = \omega_0 \left[\sqrt{1+\frac{1}{4Q^2}} - \frac{1}{2Q}\right] \approx \omega_0 \left(1 - \frac{1}{2Q}\right) \tag{8}$$

$$H(j\omega_L) = \frac{A_0}{2}(1+j) = \left|\frac{A_0}{2}\sqrt{2}\right| \angle 45. \tag{9}$$

The proposed tuning scheme is shown in Fig. 3. The two interacting loops associated with tuning of the Q and A_0 are called amplitude tuning loop and Q-tuning loop, respectively. The input signals of the amplitude and Q-tuning loops are two sinusoids at ω_0 and ω_L, respectively. The relation between these two frequencies determines the desired quality factor Q_d of the filter [see (8)].

Let us first concentrate on the amplitude tuning loop. Assuming that the input signal is $V_0\cos(\omega_0 t)$ and the filter is tuned at the desired center frequency ω_0, the peak amplitude gain A_0 can be tuned using the amplitude tuning loop shown in Fig. 3. The difference between the desired gain A_d and the actual gain A_0 is characterized by error_a which can be expressed as

$$\text{error}_a = \frac{V_0^2}{2}\left(1 - \frac{A_0}{A_d}\right). \tag{10}$$

When the amplitude tuning loop settles to its steady state, i.e., when $\text{error}_a = 0$, the peak amplitude gain A_0 at the center frequency is tuned to the desired amplitude gain of A_d. The steps to achieve A_d are indicated in Fig. 3.

Based on the -3-dB cutoff frequency information, the quality factor of the filter can be tuned to the desired Q_d using the

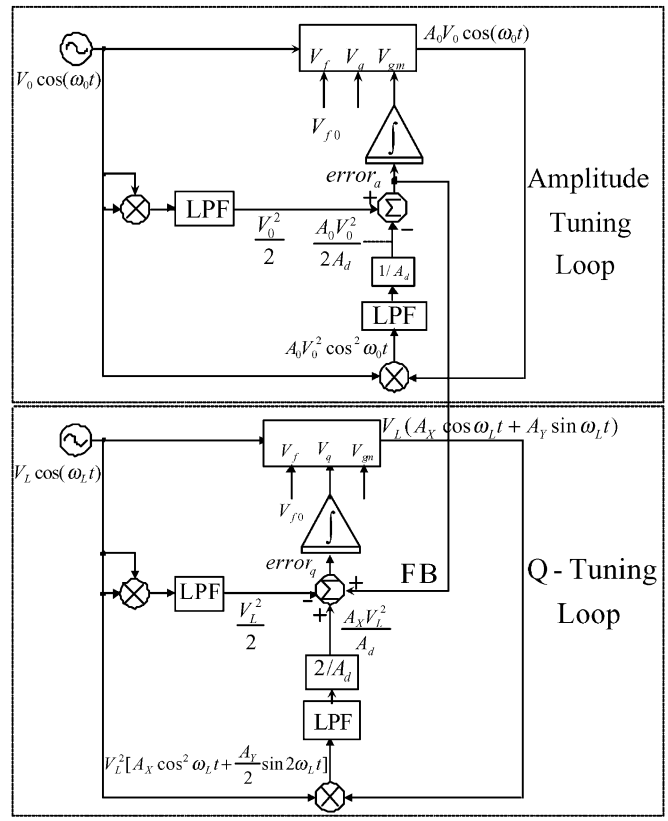

Fig. 3. Proposed schemes for amplitude and quality-factor tuning.

Q-tuning loop shown in Fig. 3. This technique relies on the fact that if $\text{Re}(H(j\omega_L)) = A_0/2$, then the correct value of Q is achieved. Note that according to (9) the output of the filter at ω_L has two components with equal amplitudes of $A_0/2$ but 45° phase difference.

However, if the proper quality factor of the filter has not already been achieved, the real part of the amplitude gain at the frequency of ω_L will differ from $A_0/2$. Let us call this gain A_X. Thus, the error of the Q-tuning loop can be expressed as

$$\begin{aligned}\text{error}_q &= \text{error}_a - \frac{V_L^2}{2}\left(1 - \frac{2A_X}{A_d}\right)\\ &= \frac{V_0^2}{2}\left(1 - \frac{A_0}{A_d}\right) - \frac{V_L^2}{2}\left(1 - \frac{2A_X}{A_d}\right).\end{aligned} \tag{11}$$

Observe from (11), when $A_0 = A_d = 2A_X$ then error_q becomes zero which means that the quality factor is appropriately tuned. Also note that the feedback signal FB in Fig. 3 does not degrade the performance of the Q-tuning loop due to mismatches in the input amplitudes V_0 and V_L. Provided that the amplitude tuning loop has been already settled to $A_0 = A_d$ and the condition $V_0 \neq V_L$ holds, if $A_X = A_d/2$ then error_q becomes zero which means that the quality factor is correctly tuned.

Let us analytically study the behavior of the Q-tuning loop. As explained above, the Q-tuning loop adapts the real part of the gain at the -3-dB cutoff frequency to be $A_0/2$. Assume that the proper value of Q has not yet been achieved. Let us call Q_a the actual filter quality factor of the filter that differs from the

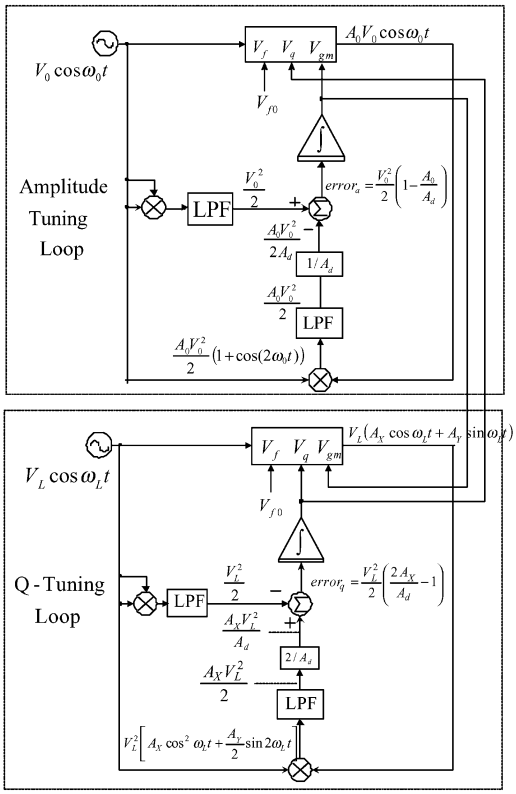

Fig. 4. Resulting amplitude and quality-factor tuning loops eliminating the feedback coupling between loops.

desired one, Q_d. The output signal of the filter in the Q-tuning loop for an input of $V_L \cos\omega_L t$ can be expressed as

$$\begin{aligned} V_o(t) &= V_L(A_X \cos\omega_L t + A_Y \sin\omega_L t) \\ &= \frac{A_0 V_L}{2} \frac{\frac{2}{Q_a^2}}{\frac{1}{Q_a^2}+\frac{1}{Q_d^2}} \cos\omega_L t \\ &\quad + \frac{A_0 V_L}{2} \frac{\frac{2}{Q_a Q_d}}{\frac{1}{Q_a^2}+\frac{1}{Q_d^2}} \sin\omega_L t. \end{aligned} \tag{12}$$

Observe from (12) that the real part of the gain at the target cutoff frequency ω_L is $A_X \neq A_0/2$. Indeed, if $Q_a < Q_d$ then $A_X > A_0/2$ and if $Q_a > Q_d$ then $A_X < A_0/2$. The deviation of the real part of the gain at ω_L, A_X, from its ideal value $A_0/2$ can be related to the relative error in the quality factor

$$A_X = \frac{A_0}{1+\frac{Q_a^2}{Q_d^2}} = \frac{A_0}{\delta_q} \tag{13}$$

$$\frac{\Delta Q_a}{Q_a} = \frac{Q_d - Q_a}{Q_a} = \sqrt{\delta_q - 1} - 1. \tag{14}$$

where $\delta_q = 1 + Q_a^2/Q_d^2$.

When the Q-tuning loop in Fig. 3 reaches its equilibrium state, δ_q becomes 2 and therefore $Q_a = Q_d$.

C. Amplitude and Q-Tuning Loops Coupling

As observed from Fig. 3, in the proposed scheme, there is a feedback signal called FB that couples the amplitude tuning and the Q-tuning loops. This coupling between the loops would force us to have two identical filters simultaneously available to implement the tuning scheme. An immediate solution would be to eliminate the feedback coupling between the two loops. This would result in the scheme shown in Fig. 4 which has two independent tuning loops. The upper tuning loop is identical to the amplitude tuning loop in Fig. 3 and forces the peak amplitude gain A_0 to settle to the desired value A_d. The lower loop in Fig. 4 controls the quality factor of the filter. The error signal error_q that controls the voltage V_q becomes $error_q = V_L^2/2(2A_X/A_d - 1)$. When error_q becomes zero the loop forces the real part of the gain at ω_L to be equal to $A_0/2$. Thus, according to (11) the actual quality factor Q_a equals the desired one Q_d.

Due to the dependence of the Q and A_0 on both V_q and V_{gm} [see (6) and (7)], the stability of the tuning scheme in Fig. 4 has to be carefully explored. Assume the amplitude control loop is not yet settled such that the overall gain is too low. Then, even if V_q is correct, the Q-tuning loop will see too small an output signal and think the Q is too large. Based on (7), V_q will then be erroneously adjusted to reduce the Q. This Q reduction through V_q will further reduce the gain A_0 [see (6)], resulting in an unstable tuning scheme.

To fix the instability problem of Fig. 4, when the amplitude tuning loop is not settled yet, the Q-tuning loop needs to know that the amplitude is too small (not yet settled). This can be accomplished by sending the amplitude error signal, error_a, to the Q-tuning loop. This is precisely the scheme proposed in Fig. 3.

An extensive analysis, shown in the next subsection, has been carried out to study the stability of the tuning schemes proposed in Figs. 3 and 4.

D. Stability Analysis

Bellow, the stability of the Q-tuning schemes shown in Figs. 3 and 4 is analyzed assuming the second-order *LC* filter shown in Fig. 2 is being tuned.

We can compute the target equilibrium values of the controlling voltages V_q and V_{gm} of the second-order filter shown in Fig. 2. Using (6) and (7) and imposing that at equilibrium $A_0 = A_d$ and $Q = Q_d$, the target equilibrium values of the controlling voltages V_q and V_{gm} of the second-order filter shown in Fig. 2 can be obtained as

$$V_{q0} = V_T + \frac{1}{\beta_q}\left(G_P - \frac{1}{Q_d}\sqrt{\frac{C}{L}}\right) \tag{15}$$

$$V_{\mathrm{gm}0} = V_T + \frac{A_d}{2\beta_m}(G_P - \beta_q(V_{q0} - V_T)). \tag{16}$$

Next, we demonstrate that both tuning systems shown in Figs. 3 and 4 with the *LC* second-order filter shown in Fig. 2 have the above values of V_{q0} and $V_{\mathrm{gm}0}$ as equilibrium point. However, the nature of the equilibrium points of both systems is very different from a stability point of view.

Let us first study the dynamics of the system shown in Fig. 4. The derivatives of the two control voltages V_{gm} and V_q in the amplitude and Q-tuning loops in Fig. 4 can be expressed as

$$\dot{V}_{\mathrm{gm}} = \frac{V_0^2}{2}\left(1 - \frac{A_0}{A_d}\right) \tag{17}$$

$$\dot{V}_q = \frac{V_L^2}{2}\left(\frac{2A_0}{A_d\delta_q} - 1\right) \tag{18}$$

where δ_q and A_0 are defined in (13) and (6), respectively.

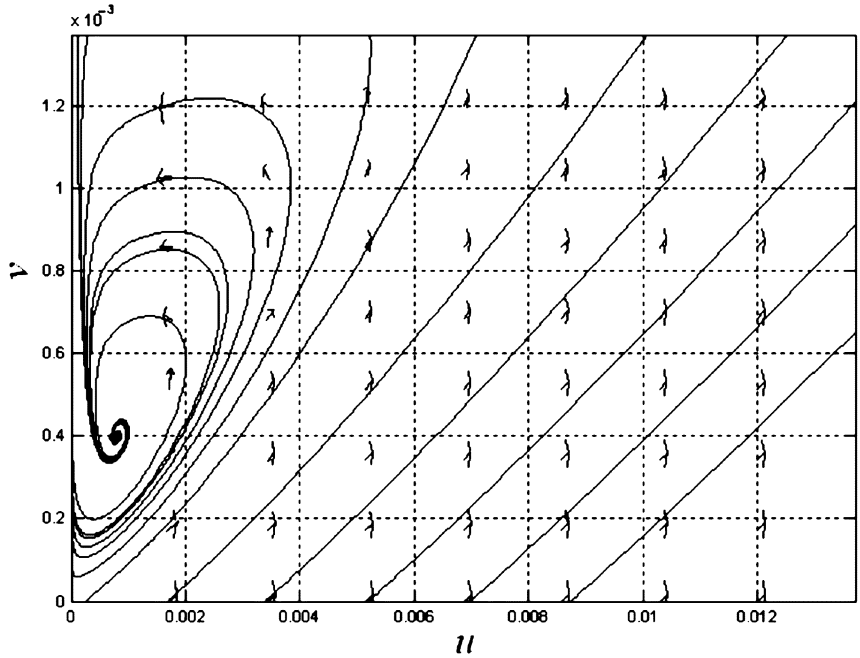

Fig. 5. Phase portrait corresponding to Fig. 4.

Substituting δ_q and A_0 for their expressions in (13) and (6) and defining the following variables $u = G_p - \beta_q(V_q - V_T), v = \beta_m(V_{\rm gm} - V_T), \dot{V}_{\rm gm} = \dot{v}/\beta_m$ and $\dot{V}_q = -\dot{u}/\beta_q$, (17) and (18) can be re-expressed as

$$\dot{u} = -K_L\left(\frac{4v}{A_d u}\frac{1}{1+\frac{C}{LQ_d^2}\frac{1}{u^2}} - 1\right) \tag{19}$$

$$\dot{v} = K_0\left(1 - \frac{2v}{A_d u}\right) \tag{20}$$

where $K_L = \beta_q V_L^2/2$ and $K_0 = \beta_m V_0^2/2$.

Equations (19) and (20) define the differential equations of a second-order nonlinear system. From these equations, we identify $u_0 = \sqrt{C/L}/Q_d$ and $v_0 = A_d\sqrt{C/L}/(2Q_d)$ as an equilibrium point, which is the same equilibrium point defined by (15) and (16). The linear approximation of the system behavior around the equilibrium point defines a stable equilibrium point. However, extensive transient simulations of the transient behavior of the nonlinear system confirm that the system does not converge to the equilibrium point for every possible initial state. These results can be confirmed graphically applying the phase portrait concept to the nonlinear system [22]. Using the phase portrait concept the qualitative behavior of the system given any initial condition can be determined.

The above technique has been applied to (19) and (20) for the following parameters: $A_d = 1, C = 1.6$ pF, $L = 3.7$ nH, $V_L = 0.9, V_0 = 1, \beta_q = 14.25$ m/Ω, $\beta_m = 1.425$ m/Ω, and $Q_d = 26$.

The phase portrait of the system is plotted in Fig. 5. Observe that the equilibrium point is a stable focus but with a reduced attraction zone. The system diverges away from the equilibrium point for a large set of possible initial conditions in the state space. In particular, the trajectories beginning with low u values converge to the equilibrium point. However, trajectories with larger u values diverge from that point. In Fig. 5, we have represented the phase portrait of all possible initial states of the system, that is, for the range of $u - v$ values that correspond to $V_q, V_{\rm gm} \in [V_T, V_{dd}]$. Values lower than V_T have not been considered as in that region (6) and (7) are no longer valid as the transistor goes into the weak inversion region.

The same approach described above has been also used to study the stability of Fig. 3. Since the amplitude tuning loop in both schemes of Figs. 3 and 4 are the same thus the expressions for $\dot{V}_{\rm gm}$ and $\dot{v}$ remain intact. However, the expressions for $\dot{V}_q$ and $\dot{u}$ are changed to the following:

$$\dot{V}_q = \frac{V_L^2}{2}\left(\frac{2A_0}{A_d\delta_q} - 1\right) + \frac{V_0^2}{2}\left(1 - \frac{A_0}{A_d}\right) \tag{21}$$

$$\dot{u} = -K_L\left(\frac{\frac{4v}{A_d u}}{1+\frac{C}{LQ_d^2}\frac{1}{u^2}} - 1\right) - \frac{\beta_q K_0}{\beta_m}\left(1 - \frac{2v}{A_d u}\right) \tag{22}$$

The same equilibrium point $u_0 = \sqrt{C/L}/Q_d$ and $v_0 = A_d\sqrt{C/L}/(2Q_d)$ can be identified from (20) and (22). Let us identify its stability behavior using the phase-portrait concept. Fig. 6 shows the phase portrait of the system defined by (20) and (22) using the same filter parameters used in Fig. 5. This figure clearly shows that there has been a change in the nature of the equilibrium point. The equilibrium point is now a stable nodal sink and the system is asymptotically stable for any possible initial condition in the state space as Fig. 6 shows.

The settling behavior of the proposed Q-tuning scheme can be studied by exploring the behavior of the equilibrium point, defined by (20) and (22), as a function of the filter parameters. It has been observed that by increasing the ratio K_L/K_O or by increasing the value of the target quality factor Q_d, the area of attraction of the equilibrium point is reduced. On the contrary the area of attraction of the equilibrium point enlarges when

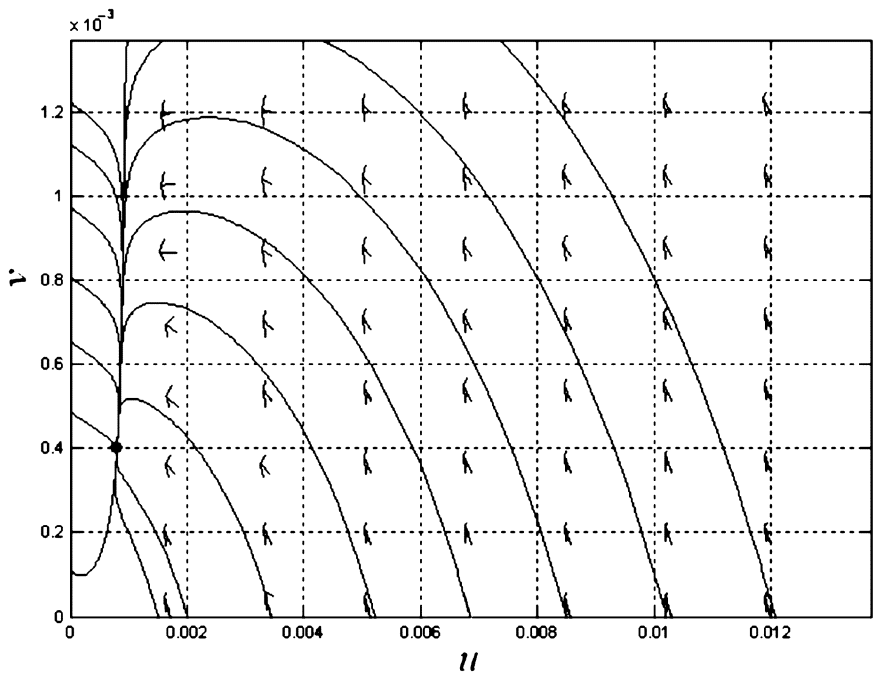

Fig. 6. Phase portrait corresponding to Fig. 3.

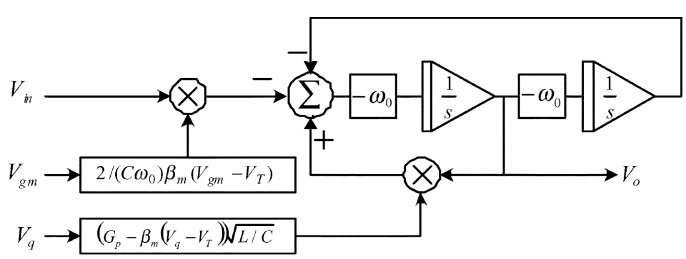

Fig. 7. Conceptual block diagram of the filter used in SIMULINK simulations.

the intrinsic quality factor of the filter increases. That is, when capacitance C is increased and/or inductance L is decreased.

The behavioral performance of the previously proposed tuning schemes in Figs. 3 and 4 have been examined using SIMULINK and their stability properties have been confirmed through SIMULINK simulations. The conceptual block diagram of the second-order *LC* bandpass filter used in the SIMULINK simulations is shown in Fig. 7.

Fig. 8 shows the simulation results of the tuning scheme proposed in Fig. 4. The simulation is done for the following target values, $\omega_0 = 13 \times 10^9$ rad/s, $A_d = 1$ and $Q = 26$. The filter parameters are the same used in the previous computations. The initial conditions of the loops were set to $V_{\rm gm} = 1$ and $V_q = 1$. For that system, the equilibrium point is $V_{\rm gm0} = 0.78$ V and $V_{q0} = 1.286$ V. In the simulation, we can observe how the system diverges from the equilibrium point as can be foreseen from the system phase portrait.

Fig. 9 shows the simulation results of the tuning scheme proposed in Fig. 3. The target values, filter parameters and initial conditions are the same ones used in the previous simulation

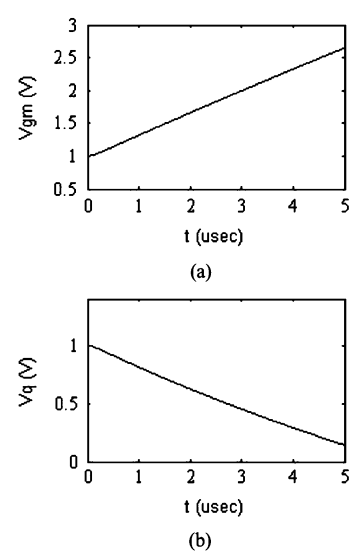

Fig. 8. SIMULINK simulation of the tuning scheme of Fig. 4. (a) $V_{\rm gm}$ versus time. (b) V_q versus time.

of Fig. 8. However, observe that in this case the system control voltages $V_{\rm gm}$ and V_q evolve towards their stable equilibrium point. Fig. 10 shows the magnitude and phase plots of the resulting tuned filter. It has the desired Q and the desired gain at the center frequency.

In Section V, it will be shown that in practice the proposed tuning scheme in Fig. 3 can be implemented, in an iterative way, using only one loop.

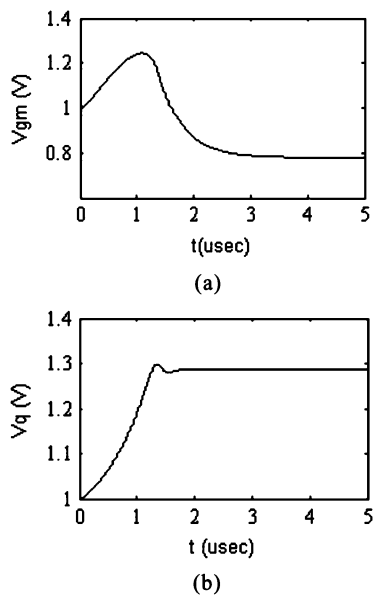

Fig. 9. SIMULINK simulation of the tuning scheme of Fig. 3. (a) $V_{\rm gm}$ versus time. (b) V_q versus time.

IV. Nonideal Effects

A. Remarks on the Effect of Parasitic Capacitances

The main parasitic capacitances in the circuit implementation of the *LC* filter are shown in Fig. 11. The overall transfer function of the filter can be expressed as

$$H(s) = \frac{V_{\rm out+}(s) - V_{\rm out-}(s)}{V_{\rm in+}(s) - V_{\rm in-}(s)} = \frac{-\frac{G_m}{C_T}\left(1 - \frac{C_{\rm id}}{G_m}s\right)s}{s^2 + \frac{G_P - G_{\rm neg}}{C_T}s + \frac{1}{LC_T}} \quad (23)$$

where $C_T = C + 4C_{od} + C_{os}$; $C_{\rm id}$ is the gate-drain capacitance of M_4-M_5 and C_{od} and C_{os} are the gate-drain and gate-source capacitances of M_2-M_3, respectively.

Comparing (3) and (23) reveals that by considering the parasitic capacitances, center frequency will decrease to $1/\sqrt{LC_T}$, which can be corrected in a frequency tuning loop, while Q will increase to $\sqrt{C_T/L}/(G_p - G_{\rm neg})$. The effect of the right half plane zero can be neglected since it is located too far away from the center frequency of the filter. Note that at the center frequency $\omega_0^2/(LC_T)$, the phase, $\theta(\omega_0)$, of the transfer function of the filter will change from 0° to $\tan^{-1}((C_{\rm id}/C_T)(1/\sqrt{LC_T}))$ and the amplitude response $\rm H(\omega_0)$ of the filter will increase by a factor of $\sqrt{1 + (C_{\rm id}/C_T)^2(1/LC_T)}$. Note that for very small $C_{\rm id}, \theta(\omega_0) \approx 0$. Since the proposed Q-tuning scheme in Fig. 3 is relying neither on the phase nor on the absolute value of the peak amplitude gain of the filter, the above variations in the phase and amplitude of the transfer function will not affect the performance of the presented scheme. In summary, our proposed tuning scheme can absorb these parasitic effects.

B. Remarks on the Effect of dc Offsets

Assume the dc offsets of the combination of the multipliers together with the LPFs in Fig. 3 can be modeled as additive terms γ. Similarly, assume the dc offsets of the summers in Fig. 3 can be modeled as additive terms θ. Including the above dc offset terms in the amplitude and Q-tuning loops of Fig. 3

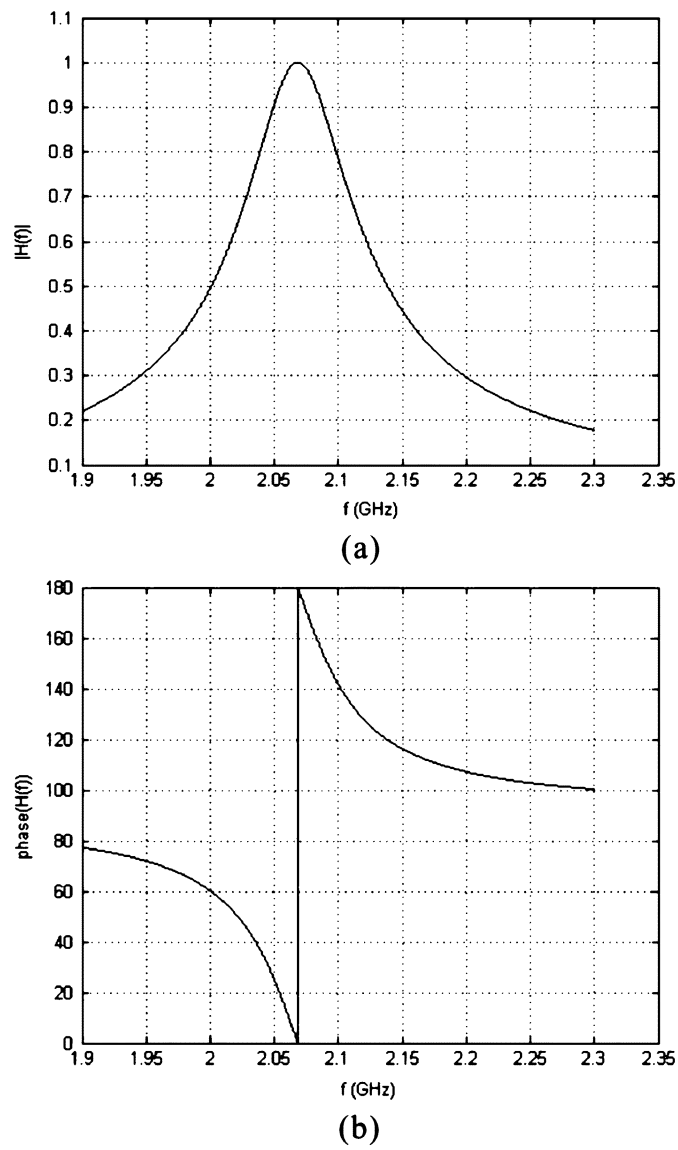

Fig. 10. (a) Magnitude and (b) phase plots of the tuned filter in Fig. 4 for $Q = 26$ and $A_d = 1$ at $f_0 = 2.07$ GHz.

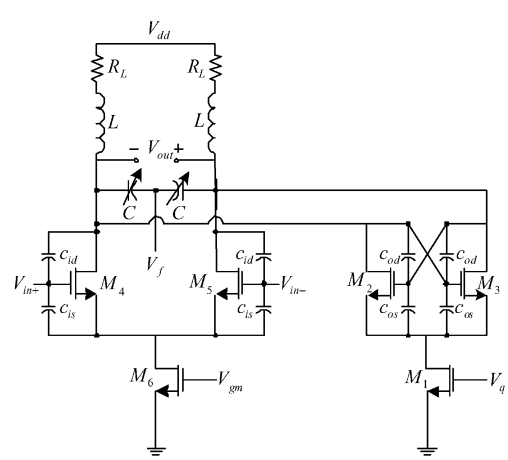

Fig. 11. Parasitic capacitances of the filter.

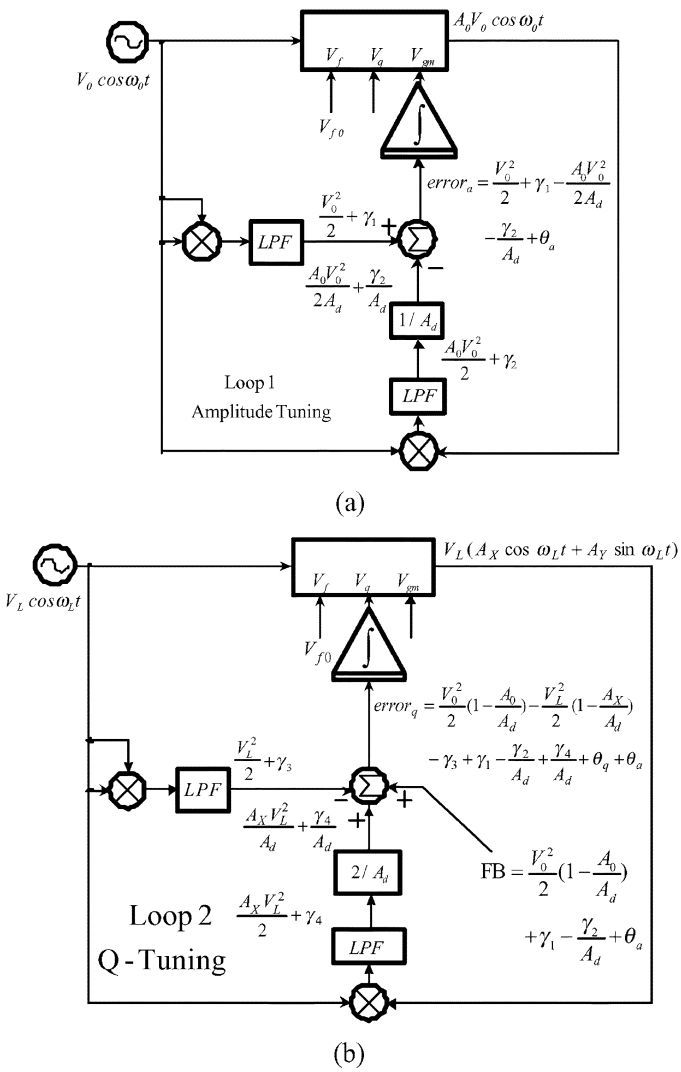

Fig. 12. Effects of the dc offsets on the Q-tuning scheme of Fig. 3 (a) Loop1 (b) Loop2.

results in the block diagram shown in Fig. 12. By following the steps shown in Fig. 12, the final error in the amplitude tuning loop including the dc offset errors can be found as

$$\text{error}_a = \frac{V_0^2}{2} - \frac{A_0}{A_d}\frac{V_0^2}{2} + \left(\gamma_1 - \frac{\gamma_2}{A_d} + \theta_a\right). \quad (24)$$

Thus, in steady state, i.e., $\text{error}_a = 0$, the relative error of the peak amplitude gain can be expressed as

$$\frac{\Delta A_0}{A_0} = \frac{A_d - A_0}{A_d} = -\frac{2}{V_0^2}\left(\gamma_1 - \frac{\gamma_2}{A_d} + \theta_a\right). \quad (25)$$

Similarly, the final error of the Q-tuning loop in Fig. 12 including the dc offset terms, can be expressed as

$$\text{error}_q = \frac{V_0^2}{2}\left(1 - \frac{A_0}{A_d}\right) - \frac{V_L^2}{2}\left(1 - \frac{A_X}{A_d}\right) - \gamma_3 + \gamma_1 - \frac{\gamma_2}{A_d} + \frac{2\gamma_4}{A_d} + \theta_q \quad (26)$$

Recall from (13) and (14) that the real part of the gain A_X at the lower cut off frequency ω_L is $A_0/\delta q$. Thus, the relative

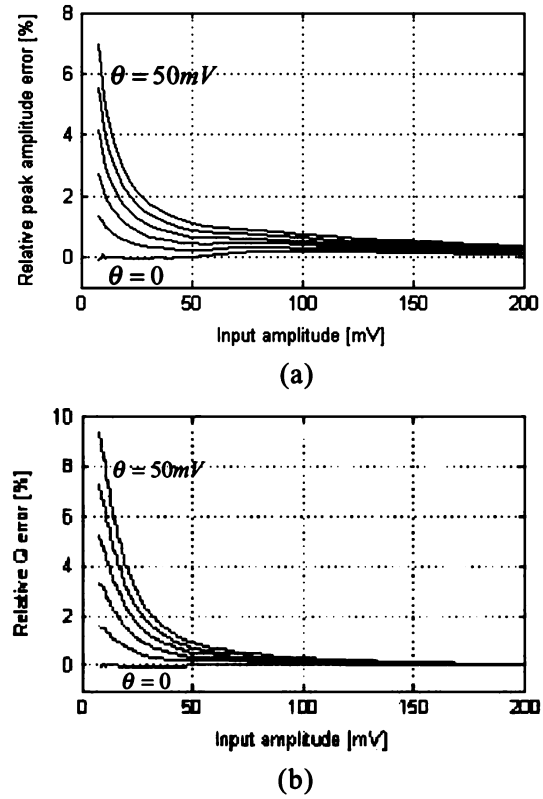

Fig. 13. Estimated errors versus θ (a) relative peak amplitude error (b) relative Q error.

Q-tuning error, including the dc offset terms, can be expressed as

$$\frac{\Delta\delta_q}{\delta_q} = \frac{-\gamma_3 + \gamma_1 - \frac{\gamma_2}{A_d} + \frac{2\gamma_4}{A_d} + \theta_q}{\frac{V_L^2}{2} + \gamma_3 - \frac{2\gamma_4}{A_d} + \theta_a - \theta_q}. \quad (27)$$

The numeric value of γ has been accurately extracted as a function of the input amplitude from the difference between the simulation and the measurement results (see Fig. 17, shown later). Assuming $A_d = 1$, the relative errors in (25) and (27) for $\theta = 0$ to $\theta = 50$ mV in steps of 10 mV have been plotted in Fig. 13. Based on these results the relative errors of the amplitude and the Q-tuning loops for $V_{\text{in}} = 50$ mV and $\theta = 50$ mV are around 1.2% and 2.5%, respectively. As Fig. 13 shows, besides minimizing the dc offsets of different blocks, by increasing the input amplitude, the relative errors in the amplitude and the Q-tuning loops can be decreased. For example, by increasing the input amplitude by 10%, for $\theta = 50$ mV and $V_{\text{in}} = 10$ mV, the above errors decrease by 0.1% and 0.12%, respectively. Furthermore, under the influence of process variations due to the mobility (10%), threshold voltage (10%) and width (5%) deviations of MOS transistors as well as 15% degradation in the sheet resistance of the top metal layer, the simulation results show that the quality factor of the filter is changed by 8% which can be tuned back using the proposed scheme.

V. TEST-CHIP MESEAUREMENT RESULTS

A prototype has been designed and fabricated in a TSMC 0.35-μm, 2-poly, four metal standard CMOS technology. The

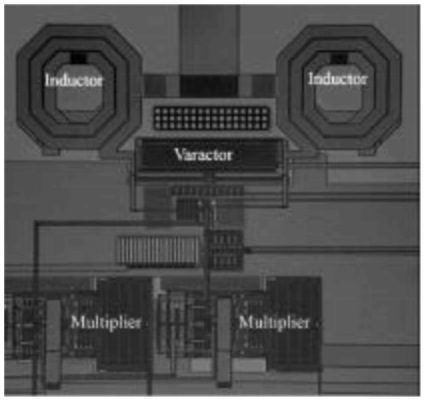

Fig. 14. Chip microphotograph.

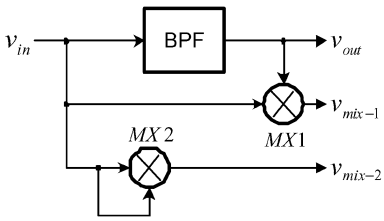

Fig. 15. Block Diagram of the fabricated chip.

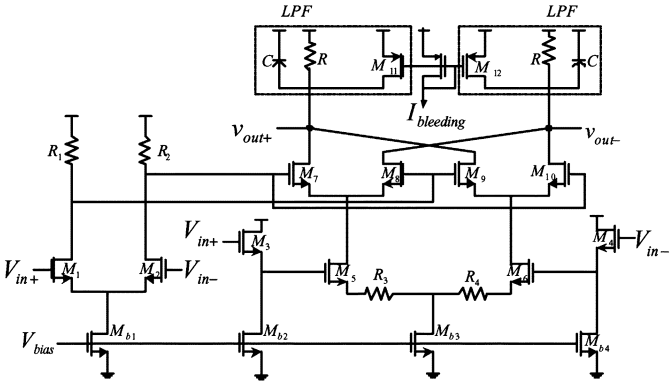

Fig. 16. Schematic of the multiplier with the *RC* LPF as its load.

microphotograph is shown in Fig. 14 which occupies a silicon area of 0.0725 mm^2 and contains a filter with two multipliers. A simple open drain output buffer is employed at the output of the filter to drive the 50 Ω load of the instrument which shows a stand-alone attenuation of around −10 dB at 1.8 GHz. Fig. 15 shows the block diagram of the fabricated prototype chip. Note that we are using only one loop (filter). Note that the input sinusoids at ω_0 and ω_L can be generated by a fractional-N synthesizer with an *LC* oscillator. However, we have used external inputs in the following experimental results.

Fig. 16 shows the transistor level implementation of the multiplier [21]. The injected current, called bleeding current, allows separate control of current flowing through the drive stage (M_1 and M_2) from the current switches (M3-M6). For the same drive bias current, bleeding reduces the current flowing through the current switches and load resistance. Thus, the flicker noise contributed by the switches is significantly reduced and allows us to use large load resistors which increase the conversion gain. Since the load of the multiplier is resistive,

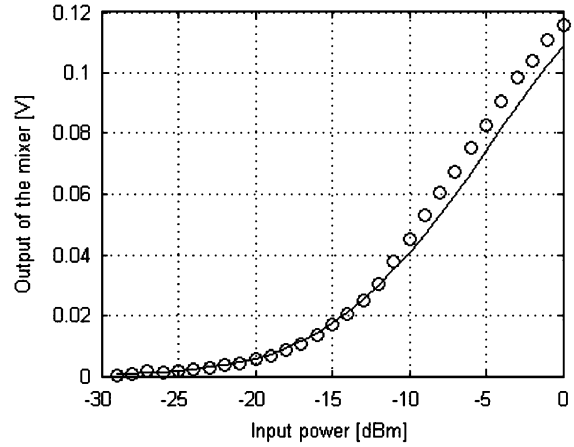

Fig. 17. DC level at the output of the multiplier MX2 in Fig. 15 as a function of the input amplitude at 2 GHz (circles: measured, solid line: simulated).

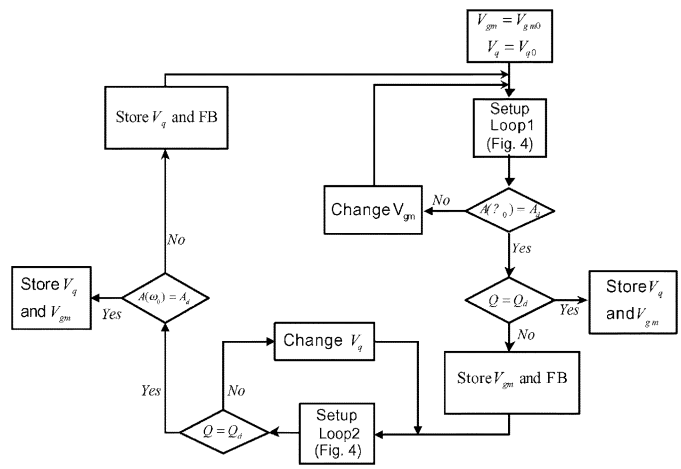

Fig. 18. Tuning algorithm using one filter.

the need of a common mode feedback circuit at the multiplier output is avoided.

It is of great importance to have exact knowledge of the dc performance of the multiplier for different input amplitudes. This has been carried out by the precise extraction of the dc output of the multiplier using the HP4156C while the test chip is shielded by the test fixture Agilent 16442A. The above setup is set to operate in the long time (1 s) mode during which the measured output is averaged over 1000 samples. Fig. 17 compares the measured and simulated dc output voltages of the multiplier with both inputs connected together. Note that the deviation of the measured data from the simulation data for amplitudes greater than −3 dBm is mainly due to the large signal operation of the multiplier which no longer provides the exact multiplication of the input amplitudes.

In this experimental prototype we chose to implement the low frequency portion of the control loops off-chip. That gives us more flexibility in the loops configuration during the testing process of the proposed procedures. However, as can be observed from Figs. 3 and 4, all the off-chip operations are just simple mathematical expressions of the signals at low frequency and thus, are appropriate for full integration of the entire tuning loop. Furthermore, the center frequency of the filter has been tuned manually throughout the following measurement results.

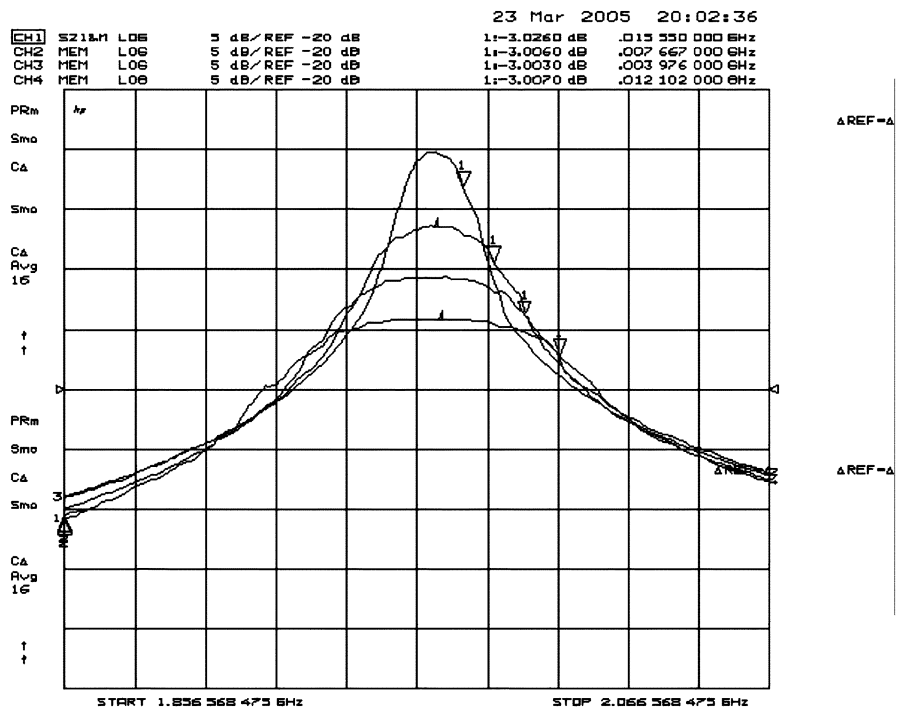

Fig. 19. Amplitude $A_0(\text{dB}) = \{-15, -10, -5, 0\}$ and Q-tuning $Q = \{60, 80, 120, 220\}$ measurement results.

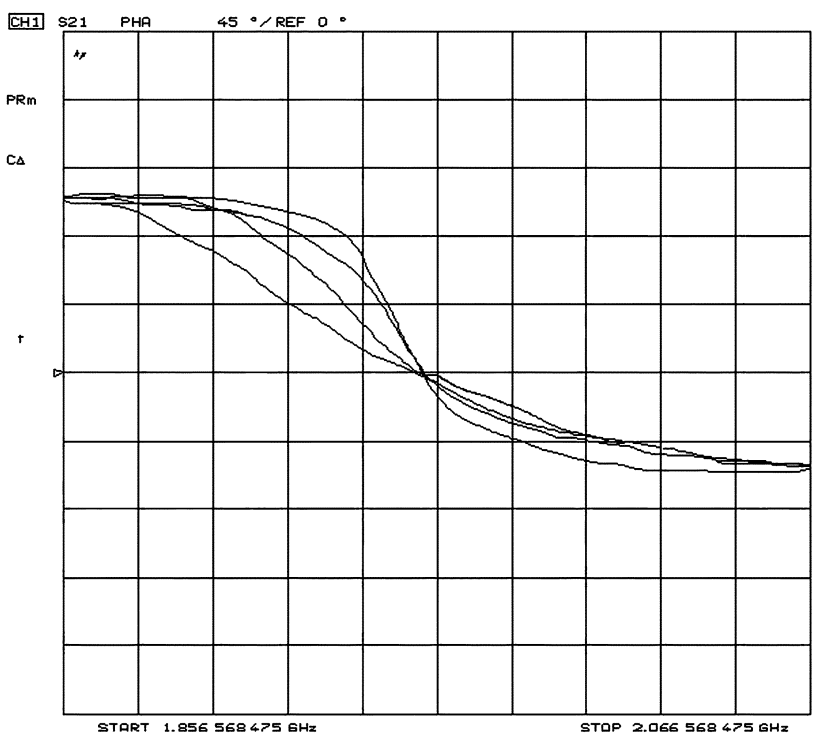

Fig. 20. Corresponding phase responses of the tuned filter in Fig. 19.

The Q-tuning procedure can be summarized as follows. Assume that for an arbitrary constant voltage V_{gm0}, the center frequency ω_0 is already set. By applying an input signal at ω_0 to the loop1 in Fig. 3, the controlling voltage V_{gm} will settle to a final voltage V_{gmf} for which error_a becomes zero i.e., $A_0 = A_d$. Then for $V_{\text{gm}} = V_{\text{gmf}}$, by applying the feedback signals FB, the Q-tuning loop in Fig. 3 (Loop2) will settle to a final control voltage of $V_q = V_{qf}$ for which error_q becomes zero i.e., $A_X = A_d/2$. In the case that we don't have two separate filters to tune the Q and the amplitude simultaneously the above procedure has to be repeated several times to get the desired amplitude and Q. Fig. 18 shows the flow chart of the tuning procedure using only one filter.

Figs. 19 and 20 show the measured frequency response of the filter using a network analyzer for five different values of A_d and Q tuned from 60 to 220 at the center frequency of 1.97 GHz. The current consumption of the filter for Q of 60 and 220 are 3.6 and 4.3 mA, respectively. In the absence of the Q-en-

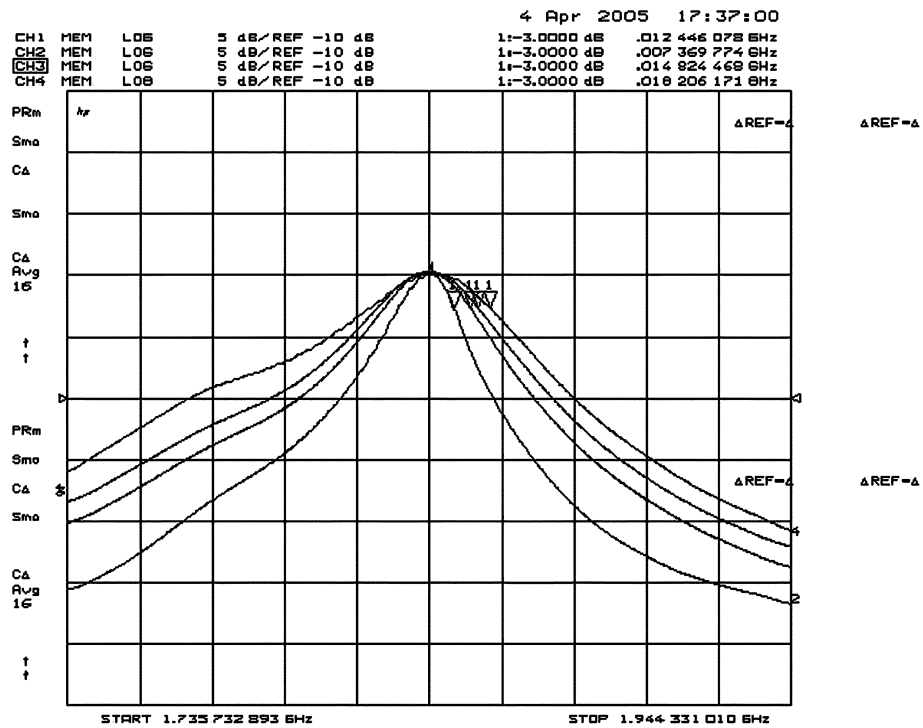

Fig. 21. Q-tuning measurement results for $Q = \{50, 60, 70, 120\}$ and fixed amplitude of $A_0 = 0$ dB.

TABLE I
SUMMARY OF EXPERIMENTAL RESULTS OF TUNING Q FOR DIFFERENT AMPLITUDES

Targeted values		Achieved values		Number of Iterations	Tuning Error (%)
Q_d	A_d (dB)	Q	A_0(dB)		Q-Tuning
60	-15	63	-14	5	4.7
80	-10	84	-11	7	4.7
120	-5	127	-7	9	5.5
220	0	246	-0.2	11	10.5

TABLE II
SUMMARY OF EXPERIMENTAL RESULTS OF TUNING Q FOR FIXED AMPLITUDE

Targeted values		Achieved values		Number of Iterations	Tuning Error (%)
Q_d	A_d(dB)	Q	A_0(dB)		Q-Tuning
50	0	51	0	5	1.9
60	0	62	-0.1	7	3.2
70	0	74	-0.1	7	5.4
120	0	125	-0.2	9	6.9

hancement technique, the measured intrinsic Q of the filter is 3. As shown in Table I which summarizes the performance of the tuning scheme, susceptibility of the filter to oscillate at very high values of Q results in higher tuning error with more iterations of the off-chip control loop.

The measured frequency response of the filter for fixed amplitude of A_d =0 dB and Q tuned from 60 to 120 is shown in the Fig. 21. In this case, since only Q is a variable in the tuning scheme, better performance has been achieved in terms of tuning error and number of iterations. The performance of the tuning loop for this case is summarized in Table II.

VI. CONCLUSION

A scheme to tune the Q and magnitude of second-order *LC* bandpass filters is presented. Using the information of the amplitude response at the center and one of the cutoff frequencies and regardless of the absolute gain of the filter at the center frequency, the proposed scheme is theoretically able to enhance the Q of the filter to an arbitrary value of Q_d such that $Q_d \geqslant R_P\sqrt{C/L}$. This property is not present in the previously reported Q-tuning schemes. In order to reduce the sensitivity of the proposed scheme to the amplitudes of the inputs, the magnitude and Q-tuning loops interact using proper correction signal FB in Fig. 3. The functionality of the tuning scheme is verified using an experimental 0.35-μm CMOS test chip. We are able to tune Q factors as high as 220 with only a 10 % error. In the present prototype, the low frequency part of the automatic tuning loops has been implemented off-chip, and the required operations of the loops have been done using software. We have chosen this approach in order to have flexibility to try different tuning strategies. However, on-chip implementation of the entire loop will not have a significant demand for power and area since they are operating at very low frequencies thus making full integration of the complete tuning loop feasible.

REFERENCES

[1] B. Razavi, *RF Microelectronics*. Englewood Cliffs, NJ: Prentice–Hall, 1998.

[2] F. Dügler, E. Sánchez-Sinencio, and J. Silva-Martinez, "A 1.3-V 5 mw fully integrated tunable bandpass filter at 2.1 GHz in 0.35-μm CMOS," *IEEE J. Solid-State Circuits*, vol. 38, no. 6, pp. 918–928, Jun. 2003.

[3] M. H. Koroglu and P. E. Allen, "*LC* notch filter for image-reject applications using on-chip inductors," *Electron. Lett.*, vol. 37, no. 5, May 2001.

[4] R. Duncan, K. W. Martin, and A. S. Sedra, "A Q-enhanced active-*RLC* bandpass filter," *IEEE Trans. Circuit Syst. II, Analog Digit. Signal Process.*, vol. 44, no. 5, pp. 341–346, May 1997.

[5] S. Pipilos, Y. P. Tsividis, J. Fenk, and Y. Papananos, "A Si 1.8 GHz *RLC* filter with tunable center frequency and quality factor," *IEEE J. Solid-State Circuits*, vol. 31, no. 10, pp. 1517–1525, Oct. 1996.

[6] D. Li and Y. Tsividis, "Design techniques for automatically tuned integrated gigahertz-range active filters," *IEEE J. Solid-State Circuits*, vol. 37, no. 8, pp. 967–977, Aug. 2002.

[7] C. Park and R. Schaumann, "Design of 4-MHz analog integrated CMOS transconductance-*C* bandpass filter," *IEEE J. Solid-State Circuits*, vol. 23, no. 4, pp. 987–996, Aug. 1988.

[8] J. M. Khoury, "Design of a 15-MHz CMOS continuous-time filter with on-chip tuning," *IEEE J. Solid-State Circuits*, vol. 26, no. 12, pp. 1988–1997, Dec. 1991.

[9] J. Silva-Martinez, M. Steyaert, and W. Sansen, "A 10.7-MHz 68-dB SNR CMOS continuous-time filter with on-chip automatic tuning," *IEEE J. Solid-State Circuits*, vol. 27, no. 12, pp. 1843–1853, Dec. 1992.

[10] R. Schaumann and M. Tan, "The problem of on-chip automatic tuning in continuous-time integrated filters," in *Proc. IEEE Int. Symp. on Circuit and Syst.*, 1989, pp. 106–109.

[11] H. Khorramabadi and P. R. Gray, "High-frequency CMOS continuous time filters," *IEEE J. Solid-State Circuits*, vol. 19, no. 6, pp. 963–967, Dec. 1984.

[12] B. Razavi, *Design of Analog CMOS Integrated Circuits*. New York: McGraw Hill.

[13] D. A. Neamen, *Electronic Circuit Analysis and Design*. New York: McGraw Hill.

[14] K. A. Kozma, D. A. Johns, and A. S. Sedra, "Automatic tuning of continuous-time integrated filter using an adaptive filter technique," *IEEE Trans. Circuit Syst. II, Analog Digit. Signal Process.*, vol. 38, no. 11, pp. 1241–1248, Nov. 1991.

[15] J. M. Stevenson and E. Sánchez-Sinencio, "An accurate quality-factor tuning Scheme for IF and high-Q continuous-time filters," *IEEE J. Solid-State Circuits*, vol. 33, no. 12, pp. 1970–1978, Dec. 1998.

[16] P. Kallam, E. Sánchez-Sinencio, and A. I. Karsilayan, "An enhanced adaptive Q-tuning scheme for a 100-MHz fully symmetric OTA-based bandpass filter," *IEEE J. Solid-State Circuits*, vol. 38, no. 4, pp. 585–593, Apr. 2003.

[17] X. He and W. B. Kuhn, "A 2.5-GHz low-power, high dynamic range, self-tuned Q-enhanced *LC* filter in SOI," *IEEE J. Solid-State Circuits*, vol. 40, no. 8, pp. 1618–1628, Aug. 2005.

[18] L. Hengesheng and A. I. Karsilayan, "An accurate automatic tuning scheme for high-Q continuous-time bandpass filters based on amplitude comparison," *IEEE Trans. Circuit Syst. II, Analog Digit. Signal Process.*, vol. 50, no. 8, pp. 415–423, Aug. 2003.

[19] T. Sumesaglam and A. I. Karsilayan, "A digital automatic tuning technique for high-order continuous-time filters," *IEEE Trans. Circuit Syst. I*, vol. 51, no. 10, pp. 1975–1984, Oct. 2004.

[20] C. DeVries and R. Mason, "A 0.18 μm CMOS, high Q-enhanced bandpass filter with direct digital tuning'','' in *Proc. IEEE Conf. Custom Integr. Circuits*, May 2002, pp. 279–282.

[21] S.-G. Lee and J.-K. Choi, "Current-reuse bleeding mixer," *Electron. Lett.*, vol. 36, pp. 696–697, Apr. 2000.

[22] H. K. Khalil, *Nonlinear Systems*. Upper Saddle River, NJ: Prentice-Hall , 2002.